

## Article

# Identification of the Benignity and Malignancy of BI-RADS 4 Breast Lesions Based on a Combined Quantitative Model of Dynamic Contrast-Enhanced MRI and Intravoxel Incoherent Motion

Wenjuan Xu <sup>1</sup> , Bingjie Zheng <sup>2</sup> and Hailiang Li <sup>2,\*</sup><sup>1</sup> Academy of Medical Science, Zhengzhou University, Zhengzhou 450001, China<sup>2</sup> Department of Radiology, The Affiliated Cancer Hospital of Zhengzhou University, Zhengzhou University, Zhengzhou 450008, China

\* Correspondence: zlyylihailiang0589@zzu.edu.cn



**Citation:** Xu, W.; Zheng, B.; Li, H. Identification of the Benignity and Malignancy of BI-RADS 4 Breast Lesions Based on a Combined Quantitative Model of Dynamic Contrast-Enhanced MRI and Intravoxel Incoherent Motion. *Tomography* **2022**, *8*, 2676–2686. <https://doi.org/10.3390/tomography8060223>

Academic Editors: Wonmo Sung and Emilio Quaia

Received: 18 August 2022

Accepted: 29 October 2022

Published: 31 October 2022

**Publisher's Note:** MDPI stays neutral with regard to jurisdictional claims in published maps and institutional affiliations.



**Copyright:** © 2022 by the authors. Licensee MDPI, Basel, Switzerland. This article is an open access article distributed under the terms and conditions of the Creative Commons Attribution (CC BY) license (<https://creativecommons.org/licenses/by/4.0/>).

**Abstract:** The aim of this study was to explore whether intravoxel incoherent motion (IVIM) combined with a dynamic contrast-enhanced magnetic resonance imaging (DCE-MRI) quantitative model can improve the ability to distinguish between benign and malignant BI-RADS 4 breast lesions. We enrolled 100 patients who underwent breast MRI at our institution and extracted the quantitative parameters of lesions with a post-processing workstation. Statistical differences in these parameters between benign and malignant BI-RADS 4 lesions were assessed using a two independent samples t-test or a Mann-Whitney U test. Binary logistic regression analysis was performed to establish five diagnostic models (model<sub>ADC</sub>, model<sub>IVIM</sub>, model<sub>DCE</sub>, model<sub>DCE+ADC</sub>, and model<sub>DCE+IVIM</sub>). Receiver operating characteristic (ROC) curves, leave-one-out cross-validation, and the Delong test were used to assess and compare the diagnostic performance of these models. The model<sub>DCE+IVIM</sub> showed the highest area under the curve (AUC) of 0.903 (95% confidence interval (CI): 0.828–0.953, sensitivity: 87.50%, specificity: 85.00%), which was significantly higher than that of model<sub>ADC</sub> ( $p = 0.014$ ) and model<sub>IVIM</sub> ( $p = 0.033$ ). The model<sub>ADC</sub> had the lowest diagnostic performance (AUC = 0.768, 95%CI: 0.672–0.846) but was not significantly different from model<sub>IVIM</sub> ( $p = 0.168$ ). The united quantitative model with DCE-MRI and IVIM could improve the ability to evaluate the malignancy in BI-RADS 4 lesions, and unnecessary breast biopsies may be obviated.

**Keywords:** breast lesion; BI-RADS; dynamic contrast-enhanced magnetic resonance imaging; intravoxel incoherent motion; diffusion weighted imaging

## 1. Introduction

In 2021, breast cancer has surpassed lung cancer to be the most common cancer in the world, accounting for a severe global burden, especially among women [1]. The identification of benign and malignant breast lesions is the most fundamental and major step in the treatment of breast diseases. As a sensitive and non-invasive examination technique, magnetic resonance imaging (MRI) plays an important role in the detection and classification of breast cancer, as well as in the observation of changes in treatment, and is widely used in clinical practice.

Breast lesions can be classified into six categories according to Breast Imaging-Reporting and Data System-Magnetic Resonance Imaging (BI-RADS-MRI) [2]. Lesions without typical signs of malignancy but with sufficiently suspicious presentation were classified as BI-RADS 4 (malignancy probability >2% but <95%) [2]. Because of the high likelihood of malignancy, the biopsy of suspicious areas is recommended in all patients with BI-RADS 4 lesions to characterize their pathology [3]. However, the wide range of malignancy possibility has also led to unnecessary histological biopsies in some patients, which is

traumatic. Therefore, further non-invasive precise diagnosis of benign and malignant BI-RADS 4 lesions is necessary.

Dynamic contrast-enhanced MRI (DCE-MRI) was proven to be a sensitive breast screening technique [4]. Some studies have investigated the morphological appearance of breast lesions on DCE-MRI, thus providing clues for the formulation of BI-RADS-MRI [5,6]. However, morphological manifestations are subjective, and some benign lesions show similar morphological features with those of breast cancer. In order to improve the ability to distinguish benign and malignant BI-RADS 4 lesions accurately, some researchers tried to explore the diagnostic value of the pharmacokinetic parameters of DCE-MRI. They found that these parameters showed initial value [7,8].

Diffusion weighted imaging (DWI) was considered a reliable adjunct to DCE-MRI, which could help visualize and quantify the random motion of water molecules in tissues, which is influenced by cell density and tissue microstructure, thus creating a contrast in tissue with no injection of contrast agents [9]. The apparent diffusion coefficient (ADC) value calculated by the single exponential model can quantitatively reflect the diffusion of water molecules in tissues. However, microcirculation perfusion and pure molecular diffusion simultaneously contribute to the ADC value, which may hinder its ability to characterize the tissue microstructure [10]. The theory of intravoxel incoherent motion (IVIM), which refers to translational movements that present a distribution of speeds in orientation and/or amplitude within a given voxel and during the measurement time, was first described by Le Bihan et al. It is based on a bi-exponential model to calculate multiple-b-value DWI data, which can simultaneously evaluate tissue diffusivity and tissue microvascular perfusion, providing richer tissue microstructural information [11].

Studies have shown that ADC-DWI and IVIM have potential application value in distinguishing benign and malignant breast lesions [12,13]. Therefore, some researchers tried to compare the diagnostic efficacy of ADC-DWI and IVIM but obtained inconsistent results [14,15]. Xiao et al. believed that the diagnostic efficacy of IVIM was higher than that of ADC-DWI [14], while Weili Ma believed that there was no statistical difference between them [15]. The potential value of combining DWI and DCE-MRI in the differential diagnosis of breast lesions has also been pointed out, but it was usually based on ADC-DWI [16], and a few related studies based on IVIM mainly combined the morphological features of DCE-MRI [17]. To our knowledge, no previous research has attempted to simultaneously assess the value of ADC-DWI, IVIM, quantitative parametric model of DCE-MRI, and their combined models in the diagnosis of BI-RADS 4 breast lesions. Therefore, this study aimed to investigate whether different DWI combined with DCE-MRI quantitative models can improve the ability to identify the malignancy of BI-RADS 4 lesions.

## 2. Materials and Methods

### 2.1. Patient Selection

Based on the following inclusion criteria, we included 100 patients with 100 breast lesions (benign: 20, malignant: 80) who underwent breast MRI at our institution from June 2016 to July 2017 and underwent subsequent treatment. Each patient was categorized according to the fifth edition of the BI-RADS-MRI guidelines. The inclusion criteria were as follows: (1) The patient was diagnosed with BI-RADS 4 breast lesions at MRI. (2) Pathological diagnosis was confirmed by needle biopsy or surgical specimen. (3) The patient had full MRI images and underwent an MRI sequences scan before biopsy. (4) The image quality of the patient met the diagnostic criteria. (5) The patient did not receive radiotherapy, chemotherapy, or surgery in the past. General clinical data and information on patients were retrospectively collected. Histopathological diagnosis of lesions was obtained by the analysis of image-guided biopsies or surgical samples. All pathological findings were defined according to the World Health Organization classification of breast lesions [18]. This study was a retrospective study that was approved by the Institutional Ethics Committee, and informed consent was waived. The study was conducted in accordance with the Declaration of Helsinki.

## 2.2. MRI Image Acquisition

MRI was acquired on a 3.0 T Skyra device (Siemens Healthcare, Erlangen, Germany) with an eight-channel bilateral breast coil in the prone position. All patients underwent breast MRI, including T1-weighted imaging, T2-weighted imaging, DCE-MRI, and transverse multiple-b DWI. DCE-MRI was performed using time-resolved angiography with interleaved stochastic trajectories sequence and the following parameters: the repetition time (TR), 4.18 ms; the echo time (TE), 1.31 ms; field of view (FOV),  $640 \times 560 \text{ mm}^2$ ; slice thickness, 2.0 mm; no gap; matrix,  $320 \times 249$ ; flip angle,  $12^\circ$ ; temporal resolution, 7.84 s/phase; and acquisition time (TA), 5 min and 33 s. At the beginning of the fourth DCE-MRI frame acquisition, an intravenous bolus injection of 0.2 mmol/kg Gd-DTPA-BMA (Omni-Scan, GE Healthcare, Dublin, Ireland) was administered at a rate of 2.5 mL/s, followed by a 20 mL saline flush.

Transverse multiple-b DWI was acquired using an ISHIM sequence before the DCE-MRI. Nine b values were used: 0, 25, 50, 75, 100, 200, 400, 600, 800  $\text{s}/\text{mm}^2$ . The corresponding parameters were as follows: TR, 4209 ms; TE, 58 ms; FOV,  $640 \times 560 \text{ mm}^2$ ; slice thickness, 4.0 mm; matrix,  $128 \times 67$ ; slice-gap, 4.4 mm; flip angle,  $90^\circ$ ; bandwidth, 2440 Hz/pixel; 1 average. The total scan time for the multiple-b DWI sequence was 3 min 34 s.

## 2.3. Image Analysis

ADC values of breast lesions were calculated from a single exponential fitting model of signal intensities at  $b = 0$  and  $b = 800 \text{ s}/\text{mm}^2$ :

$$S_b = S_0 \cdot \exp^{-b\text{ADC}} \quad (1)$$

The pure diffusion coefficient  $D$ , the perfusion-related diffusion coefficient  $D^*$  and the perfusion fraction  $f$  were obtained by the following bi-exponential fitting model as described by Le Bihan et al. [19]:

$$S_b/S_0 = (1 - f) \cdot \exp^{-b \cdot D} + f \cdot \exp^{-b(D+D^*)} \quad (2)$$

where  $S_b$  represents the signal intensity with a specific b value, and  $S_0$  represents the signal intensity without a diffusion gradient. Since the contribution of  $D^*$  to signal attenuation is negligible at high b values ( $b > 200 \text{ s}/\text{mm}^2$ ), a single exponential fitting equation ( $S_b = S_0 \cdot \exp^{-bD}$ ) was used to determine  $D$ . Then, with the result  $D$  as a fixed parameter,  $D$  is applied to the above bi-exponential equation (Equation (2)), and  $D^*$  and  $f$  are derived using all the values of b.

All post-processing operations of DWI images were performed on a workstation (Advantage Workstation 5.0, GE Healthcare, Saint Louis, MO, USA) and were analyzed with FuncTool 9.4.05 MADC and ADC software, respectively, and  $D$ ,  $D^*$ ,  $f$ , ADC parameter maps were obtained. Two radiologists (BZ and WX, with 10 and 2 years of experience in breast image interpretation, respectively), blinded to pathological findings, clinical data, and other imaging findings, reviewed all images and delineated regions of interest (ROIs), respectively. With T2WI and DCE-MRI images as references, they determined the extent of the lesion on the corresponding IVIM and ADC parameter maps and then manually delineated the ROI along the lesion edge at the slice of the maximum lesion diameter. Similar to previous studies [17], areas of apparent cystic lesions, necrosis, calcification, and hemorrhage were avoided. Subsequently, the software automatically calculated the quantitative parameters  $D$ ,  $D^*$ ,  $f$ , ADC within the ROI.

The same two radiologists analyzed DCE-MRI images with Omni-Kinetics software. Based on the Extended Tofts Linear mode, the software automatically obtained pharmacokinetic parameter maps. ROIs, which were as consistent as possible with the ROIs on the IVIM and ADC images, were drawn by radiologists at the early enhancement phase (Figure 1). Then the pharmacokinetic parameters ( $K^{\text{trans}}$ ,  $K_{\text{ep}}$ ,  $V_e$ ) of the ROI were calculated automatically by the software.

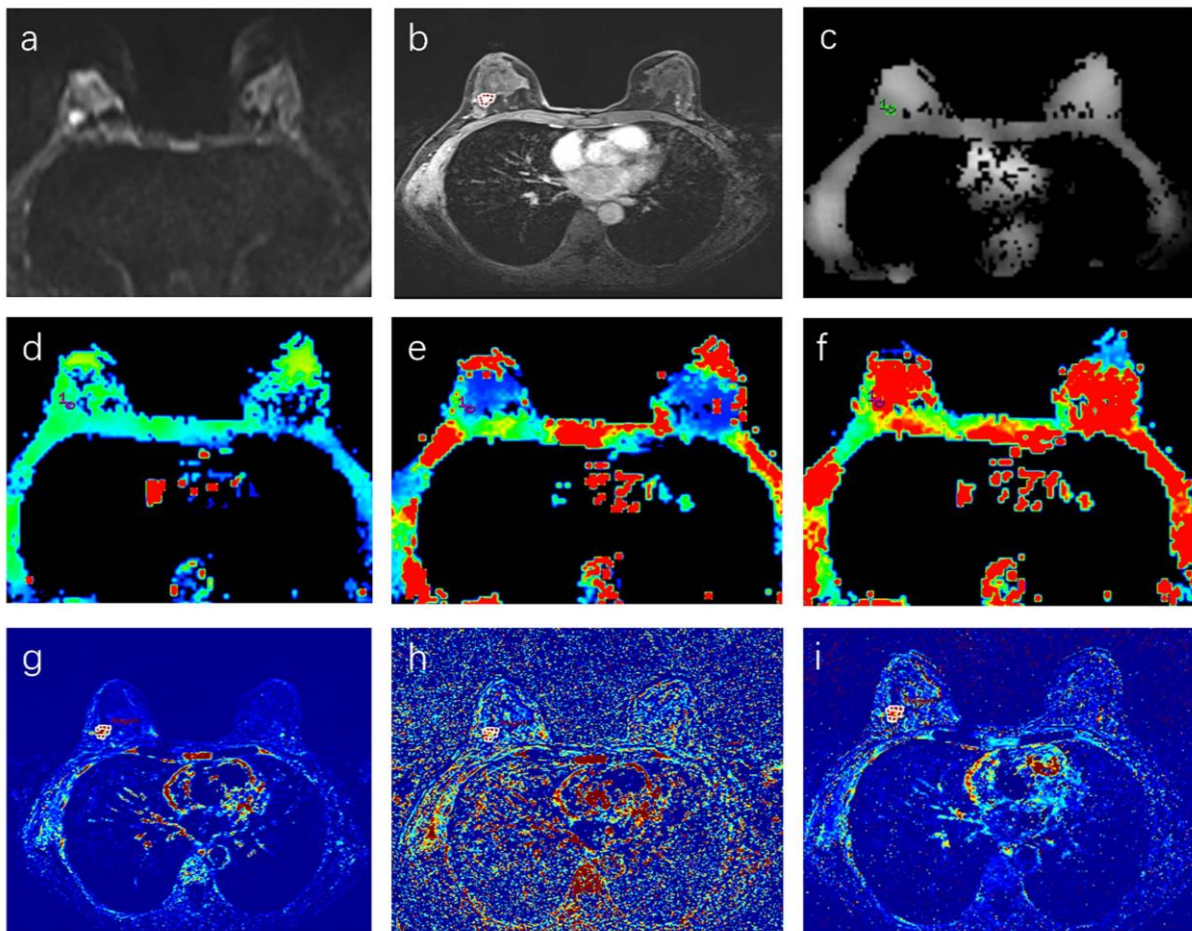


**Figure 1.** (a–i) A 46-year-old woman with a malignant BI-RADS 4 lesion in the right breast. (a) Diffusion-weighted imaging at  $b = 800 \text{ mm}^2/\text{s}^2$ . (b) Dynamic contrast-enhanced imaging, (c) ADC map, (d) D map, (e)  $D^*$  map, (f)  $f$  map, (g)  $K^{\text{trans}}$  map, (h)  $K_{\text{ep}}$  map, (i)  $V_e$  map. The circle stands for the delineated ROI.

#### 2.4. Statistical Analysis

Statistical analysis was performed on IBM SPSS (v26.0; Chicago, IL, USA), MedCalc (v19.6; Ostend, Belgium) and R (version 4.2.1). The intraclass correlation coefficient (ICC) was used to evaluate the agreement of the quantitative parameters measured by the two radiologists. Data were analyzed for normality with the Shapiro–Wilk test, followed by an analysis of variance homogeneity with the Levene test. A two independent samples  $t$ -test or a Mann–Whitney U test was used to evaluate the statistical differences of quantitative parameters between benign and malignant lesions. Binary logistic regression analysis (Method: Forward: LR) was performed to establish five diagnostic models (model\_ADC, model\_IVIM, model\_DCE, model\_DCE+ADC, and model\_DCE+IVIM) with a variable selection criterion of  $p < 0.05$ . The receiver operating characteristic (ROC) curves, leave-one-out cross-validation (LOOCV), and the Delong test were used to evaluate and compare the diagnostic performance of these models.

### 3. Results

#### 3.1. Patient Characteristics

We screened 176 consecutive patients defined as BI-RADS 4 at MRI, excluding 12 patients without IVIM sequences, 52 patients who underwent needle biopsy before MRI, 5 patients whose tumors were too small to accurately delineate the ROI, and 7 patients with incomplete images. Finally, 100 patients with 100 breast lesions (benign: 20, malignant: 80) were included in this study, and their characteristics are summarized in Table 1. The mean age of all patients was 47.4 years, with a range of 26–73 years. The mean age

of patients in the benign lesion group was significantly lower than that in the malignant lesion group ( $p = 0.001$ ).

**Table 1.** Basic clinical information of enrolled patients.

Parameter	Number of Patients
Benign lesions	20
Mean age (years)	40.8 (26–61)
Histological result	
Fibroadenoma	9
Granulomatous mastitis	3
Adenomatosis	3
Phyllodes tumor (benign)	3
Fibrocystic change	2
Malignant lesions	80
Mean age (years)	49.0 (29–73)
Histological result	
Ductal carcinoma in situ	8
Invasive ductal carcinoma	62
Invasive lobular carcinoma	5
Mucinous carcinoma	3
Paget's disease	1
Metaplastic carcinoma	1

Data in parentheses are range.

### 3.2. Consistency Test

After the inter-observer agreement analysis of all parameters, it was found that the ICCs of all parameters was greater than 0.82 except for  $D^*_{\min}$  (ICC = 0.419) and  $K_{ep_{\min}}$  (ICC = 0.701), and the details are shown in Table 2, indicating that these parameters measured by the two radiologists were in good agreement. Therefore, parameters in good agreement were subjected to subsequent statistical analysis.

**Table 2.** Consistency test results for each parameter.

Parameter	ICC	Parameter	ICC	Parameter	ICC
$K^{\text{trans}}_{\min}$	0.875	$V_{e_{\min}}$	0.844	$D^*_{\min}$	0.419
$K^{\text{trans}}_{\max}$	0.865	$V_{e_{\max}}$	0.876	$D^*_{\max}$	0.867
$K^{\text{trans}}_{\text{median}}$	0.951	$V_{e_{\text{median}}}$	0.991	$f_{\text{mean}}$	0.913
$K^{\text{trans}}_{\text{mean}}$	0.960	$V_{e_{\text{mean}}}$	0.981	$f_{\min}$	0.865
$K_{ep_{\min}}$	0.701	$D_{\text{mean}}$	0.913	$f_{\max}$	0.821
$K_{ep_{\max}}$	0.946	$D_{\min}$	0.911	$ADC_{\text{mean}}$	0.999
$K_{ep_{\text{median}}}$	0.906	$D_{\max}$	0.916	$ADC_{\min}$	0.997
$K_{ep_{\text{mean}}}$	0.919	$D^*_{\text{mean}}$	0.954	$ADC_{\max}$	0.997

ICC, intraclass correlation coefficient. "D\*" is the perfusion-related diffusion coefficient calculated by the post-processing software.

### 3.3. DWI and DCE-MRI Quantitative Parameters in Benign and Malignant Breast Lesions

The  $D_{\text{mean}}$ ,  $D_{\min}$ ,  $D_{\max}$ ,  $D^*_{\text{mean}}$ , and  $D^*_{\max}$  values of malignant lesions were significantly lower than those of benign lesions (all  $p < 0.05$ ), while the values of  $f_{\text{mean}}$  and  $f_{\min}$  were significantly higher than those of benign lesions ( $p = 0.035$ ,  $0.009$ , respectively). The ADC-related parameter values of benign lesions were significantly higher than those of malignant lesions (all  $p < 0.001$ ), but the DCE-related pharmacokinetic parameters such as  $K^{\text{trans}}_{\max}$ ,  $K_{ep_{\max}}$ ,  $K_{ep_{\text{median}}}$ , and  $K_{ep_{\text{mean}}}$  values were significantly lower than those of malignant lesions (all  $p < 0.05$ ). No significant differences in  $V_e$ -related parameters were observed between benign and malignant lesions. More detailed data are shown in Table 3.

**Table 3.** Comparison of parameters between benign and malignant lesions.

Parameter	Benign Lesions (n = 20)	Malignant Lesions (n = 80)	p Value
D <sub>mean</sub> (×10 <sup>-3</sup> mm <sup>2</sup> /s)	1.41 ± 0.27	1.07 ± 0.26	<0.001 #
D <sub>min</sub> (×10 <sup>-3</sup> mm <sup>2</sup> /s)	1.21 (1.02,1.60)	0.93 (0.74,1.11)	<0.001
D <sub>max</sub> (×10 <sup>-3</sup> mm <sup>2</sup> /s)	1.51 ± 0.25	1.18 ± 0.26	<0.001 #
D* <sub>mean</sub> (×10 <sup>-3</sup> mm <sup>2</sup> /s)	27.05 (10.98,78.65)	15.20 (8.37,28.05)	<b>0.032</b>
D* <sub>min</sub> (×10 <sup>-3</sup> mm <sup>2</sup> /s)	9.88 (5.70,31.33)	7.97 (4.87,13.38)	0.289
D* <sub>max</sub> (×10 <sup>-3</sup> mm <sup>2</sup> /s)	44.65 (21.05,29.38)	22.50 (13.20,46.30)	<b>0.025</b>
f <sub>mean</sub> (%)	11.00 (5.17,15.48)	13.70 (11.20,19.70)	<b>0.035</b>
f <sub>min</sub> (%)	7.44 (2.89,11.20)	10.25 (7.94,12.55)	<b>0.009</b>
f <sub>max</sub> (%)	16.90 (9.59,24.48)	17.60 (14.53,29.15)	0.252
ADC <sub>mean</sub> (×10 <sup>-3</sup> mm <sup>2</sup> /s)	1.52 ± 0.25	1.28 ± 0.25	<b>0.001 #</b>
ADC <sub>min</sub> (×10 <sup>-3</sup> mm <sup>2</sup> /s)	1.46 ± 0.26	1.22 ± 0.25	<b>0.001 #</b>
ADC <sub>max</sub> (×10 <sup>-3</sup> mm <sup>2</sup> /s)	1.58 ± 0.25	1.35 ± 0.25	<b>0.001 #</b>
K <sup>trans</sup> <sub>min</sub> (min <sup>-1</sup> )	0.06 (0.03,0.09)	0.06 (0.03,0.18)	0.558
K <sup>trans</sup> <sub>max</sub> (min <sup>-1</sup> )	0.42 (0.15,1.71)	1.02 (0.46,2.38)	<b>0.011</b>
K <sup>trans</sup> <sub>median</sub> (min <sup>-1</sup> )	0.19 (0.09,0.60)	0.35 (0.15,0.75)	0.095
K <sup>trans</sup> <sub>mean</sub> (min <sup>-1</sup> )	0.20 (0.09,0.66)	0.39 (0.16,0.83)	0.064
K <sub>ep_min</sub> (min <sup>-1</sup> )	0.01 (0.00,0.06)	0.000 (0.00,0.12)	0.571
K <sub>ep_max</sub> (min <sup>-1</sup> )	0.75 (0.46,0.97)	1.80 (1.15,3.07)	<0.001
K <sub>ep_median</sub> (min <sup>-1</sup> )	0.28 (0.19,0.49)	0.52 (0.37,0.75)	<b>0.001</b>
K <sub>ep_mean</sub> (min <sup>-1</sup> )	0.31 (0.19,0.50)	0.61 (0.39,0.82)	<0.001
V <sub>e_min</sub>	0.11 (0.00,0.32)	0.00 (0.00,0.28)	0.222
V <sub>e_max</sub>	1.00 (1.00,1.00)	1.00 (1.00,1.00)	0.964
V <sub>e_median</sub>	0.75 (0.38,1.00)	0.68 (0.33,0.98)	0.632
V <sub>e_mean</sub>	0.73 (0.41,0.93)	0.68 (0.38,0.87)	0.477

Normally distributed data are presented as mean±standard deviation, and non-normal data are presented as median (interquartile range). The *p* value was calculated with the two independent samples *t*-test (#) or a Mann-Whitney U test. *p* values < 0.05 are presented in bold.

The ROC curves of the diagnostic performance of each multivariate model are shown in Figure 2. The AUC, 95% CI, standard error, sensitivity, specificity, accuracy, and *p*-values of these models are shown in Table 4. The diagnostic performance of these models was compared by the DeLong test, and the results with significant differences are shown in Table 5. Compared with the model<sub>ADC</sub> (AUC = 0.768, 95%CI: 0.672–0.846), the model<sub>IVIM</sub> (AUC = 0.826, 95%CI: 0.737–0.894, *p* = 0.168 by DeLong test) improved the diagnostic performance of BI-RADS 4 lesions, but the difference was not significant. The diagnostic efficiency of model<sub>DCE+IVIM</sub> was the highest, with an AUC of 0.903, and the sensitivity and specificity were 87.5% and 85%, respectively.

**Table 4.** Diagnostic performance of the models.

Model	Variables	AUC	Standard Error	95% Confidence Interval		Accuracy (%)	Sensitivity (%)	Specificity (%)
				Lower Bound	Upper Bound			
model <sub>ADC</sub>	ADC <sub>min</sub>	0.768	0.063	0.672	0.846	0.789	75.00	75.00
model <sub>IVIM</sub>	D <sub>mean</sub>	0.826	0.044	0.737	0.894	0.820	72.50	80.00
model <sub>DCE</sub>	K <sub>ep_max</sub>	0.823	0.056	0.734	0.892	0.793	78.75	85.00
model <sub>DCE+ADC</sub>	K <sub>ep_max</sub> , ADC <sub>min</sub>	0.852	0.049	0.768	0.915	0.789	86.25	75.00
model <sub>DCE+IVIM</sub>	K <sub>ep_max</sub> , D <sub>mean</sub>	0.903	0.037	0.828	0.953	0.789	87.50	85.00

**Table 5.** Models with significant difference in ROC curves after the Delong test.

Model	Standard Error	<i>p</i> Value
model_DCE+IVIM vs. model_IVIM	0.036	0.033
model_DCE+IVIM vs. model_ADC	0.055	0.014

ROC, receiver operating characteristic.

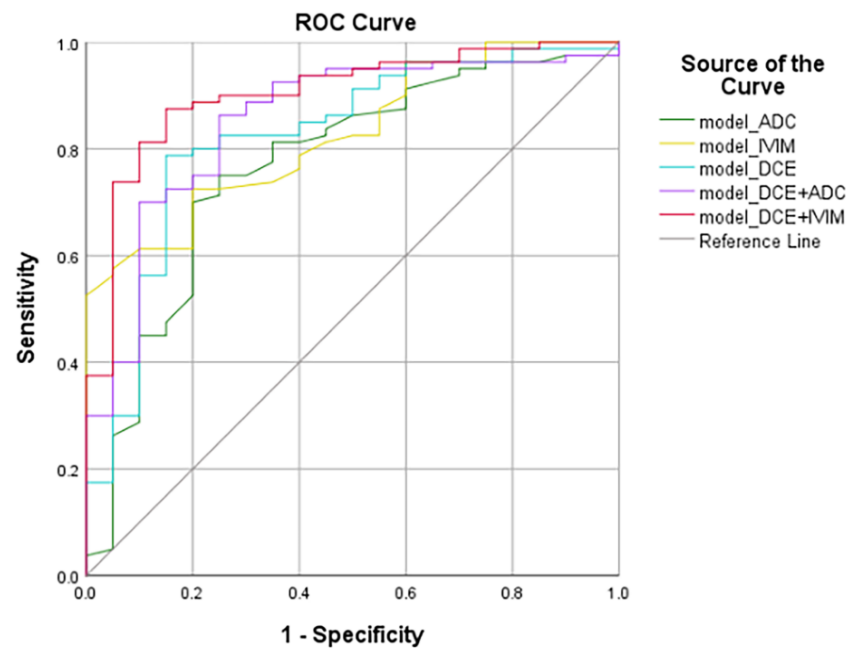


**Figure 2.** ROC curves of the models. The ROC curves were generated by models based on: ADC–DWI, IVIM, DCE–MRI, DCE–MRI + ADC–DWI, DCE–MRI + IVIM. ROC, receiver operating characteristic.

#### 4. Discussion

This study analyzed the role of ADC–DWI, IVIM, and DCE–MRI in identifying the benignity and malignancy of BI-RADS 4 breast lesions. Combining the quantitative variables of these sequences, this study concluded that the single IVIM and the DCE model showed better diagnostic performance compared to the single ADC–DWI model, although the difference was not significant. The combined model of IVIM and DCE–MRI could improve the sensitivity and specificity of diagnosis most and help patients avoid unnecessary breast biopsy.

Breast MRI has the advantages of good soft tissue resolution and no radiation [20,21]. The likelihood of BI-RADS 4 breast lesions being malignant ranged from 2% to 95%, but the actual positive predictive value of breast lesions ranged from 25.7% to 59.2% [22–24]. Since MRI is insensitive to microcalcifications, it can easily lead to false-negative diagnoses [25], and morphological assessments are highly subjective, which may lead to the overdiagnosis of patients. Therefore, we combined the quantitative variables of DCE–MRI, IVIM, and ADC–DWI, established multiple quantitative models, and compared their diagnostic performance to provide radiologists and oncologists with a more reliable quantitative assessment tool.

In multivariate logistic regression analysis,  $ADC_{min}$ ,  $D_{mean}$ , and  $K_{ep_{max}}$  were found to be independent predictors of breast malignancy. ADC values can be used to estimate tumor biological characteristics such as water content, tissue cell density, vessel density, and cell membrane integrity [11]. The  $ADC_{min}$  value of malignant lesions was lower than that of benign lesions, which was the same as the previous research results [26]. This might be attributed to the continuous proliferation of tumor cells, the increase in the synthesis of macromolecular substances in the cytoplasm, the release of a large amount of necrotic substances, the reduction of extracellular space, the increase of bound water content, and the restricted diffusion of free water molecules [27]. A meta-analysis showed that the ADC

value for distinguishing between benign and malignant breast lesions range from 0.92 to  $1.61 \times 10^{-3} \text{ mm}^2/\text{s}$  [28]. In this study, the optimal threshold for  $\text{ADC}_{\text{min}}$  was  $1.31 \times 10^{-3} \text{ mm}^2/\text{s}$ , which is consistent with previous findings.

$D$  is the diffusion coefficient of pure water in the tissue. Malignant breast lesions are associated with the limited diffusion of water molecules due to rapid proliferation, high density, and the shrinking of the extracellular space of tumor cells. The  $D^*$  value and the  $f$  value mainly reflect the state of blood perfusion. In this study, the values of  $D$ -related parameters,  $D^*_{\text{mean}}$ , and  $D^*_{\text{max}}$ , in malignant lesions were significantly lower than those in benign lesions (all  $p < 0.05$ ), while  $f_{\text{min}}$  and  $f_{\text{mean}}$  were significantly higher ( $p = 0.009$ ;  $p = 0.035$ ), which was consistent with the results of Yichuan Ma [29]. However, there were also some different opinions; Nan Meng believed that the  $D^*$  value of breast cancer was higher than that of benign lesions [30], while Liang et al. believed that the  $D^*$  value of benign and malignant lesions was not statistically different [31]. The reason for this discrepancy may be patient selection bias: fibroadenoma and inflammation with hyperperfusion in this study accounted for 60% of benign lesions, making  $D^*$  and  $f$  of benign lesions overlap with malignant lesions. In addition, the  $D^*$  value is affected by age and menstrual status. The  $D^*$  value of the normal breast tissue of postmenopausal subjects is significantly lower than that of premenopausal subjects, and the premenopausal  $D^*$  value (low and middle age groups) fluctuates with the menstrual cycle [32]. However, potential influencing factors such as age and menstrual cycle were not considered in this study, which might have a certain impact on the accuracy of the  $D^*$  value.

DCE-MRI can characterize the complex microcirculation in living tissue and provide quantitative information on vascular permeability and angiogenesis. Higher  $K^{\text{trans}}$  and  $K_{\text{ep}}$  values reflect higher microvascular blood flow, vascular density, and vascular permeability in diseased tissue [33]. In this study, the  $K^{\text{trans}}_{\text{max}}$  and  $K_{\text{ep}}$ -related parameter values of malignant lesions were significantly higher than those of benign lesions, which was consistent with the results of previous studies [34]. This may be attributed to the increased leakage of contrast agents due to incomplete vascular endothelial cells and high vascular permeability in malignant breast lesions [35]. In addition, local hypoxia and necrotic sites in malignant lesions release angiogenic cytokines, leading to increased angiogenesis and microvascular leakage [36]. The  $K_{\text{ep}_{\text{max}}}$  value was considered an independent predictor of malignancy in the logistic regression analysis, while the  $K^{\text{trans}}$  value was not included, possibly because  $K^{\text{trans}}$  value was potentially affected by conditions such as cardiac output and hypertension that affect blood perfusion [36].

After the DeLong test, we found that the diagnostic performance of the model  $_{\text{IVIM}}$  was higher than that of the model  $_{\text{ADC}}$ , but their differences did not reach statistical significance, which was the same as the findings of Iima M and Baxter GC [37,38], who recommended using ADC-DWI in the clinic to distinguish benign from malignant lesions in order to reduce image acquisition time. However, the conclusion of Xiao et al. was different. They believed that the diagnostic performance of IVIM was significantly higher than ADC-DWI [14]. We speculated that these differences may be due to the study population, the size and number of the  $b$ -value, ROI location, and post-processing software. The diagnostic efficiency of the model  $_{\text{DCE+IVIM}}$  was significantly higher than that of the model  $_{\text{ADC}}$  and model  $_{\text{IVIM}}$  and higher than the model  $_{\text{DCE+ADC}}$  and model  $_{\text{DCE}}$  but did not reach statistical significance, suggesting that the combination of IVIM and DCE-MRI quantitative parameters could better predict the malignancy of BI-RADS 4 breast lesions, which might be attributed to the combination of assessing microvascular perfusion and cell proliferation. Although the acquisition time of IVIM was longer, making it difficult to apply in clinics, some studies suggested that simplified IVIM could also achieve the same diagnostic effect as conventional IVIM [39]. However, there was no research to compare the diagnostic effect of the simplified model  $_{\text{DCE+IVIM}}$  with that of the conventional model  $_{\text{DCE+IVIM}}$ . We will try to discuss this in the next step.

There were some limitations of this study: (1) This study was a single-center retrospective study. The sample size of benign lesions was small, and fibroadenomas were the

main ones, so there might be sampling bias. (2) In this study, the manual delineation of ROI might have measurement errors. However, in the consistency analysis of this study, it was found that the consistency of manual delineation was good. (3) Factors such as patient age and menstrual cycle were not considered when patients were included in the study. All of the above need to be further studied by increasing the sample size in the follow-up process.

## 5. Conclusions

In conclusion, the model built with DCE–MRI and IVIM quantitative parameters seems to be a more reliable tool for evaluating the malignancy in BI-RADS 4 lesions compared to the single ADC–DWI and IVIM models.

**Author Contributions:** Conceptualization, W.X.; data curation, W.X. and B.Z.; formal analysis, W.X.; project administration, H.L.; resources, H.L.; supervision, B.Z. and H.L.; writing—original draft, W.X.; writing—review and editing, B.Z. and H.L. All authors have read and agreed to the published version of the manuscript.

**Funding:** This research was funded by the Health Commission of Henan Province, funding number “LHGJ20210207”.

**Institutional Review Board Statement:** The study was conducted in accordance with the Declaration of Helsinki and approved by the Institutional Review Board of the Affiliated Cancer Hospital of Zhengzhou University & Henan Cancer Hospital (protocol code “2022-KY-0005” and date of approval “2022.3.15”).

**Informed Consent Statement:** Patient consent was waived because this study utilized human material or data with identifiable information, the subject could no longer be located, and the research project did not involve personal privacy or commercial interests.

**Conflicts of Interest:** The authors declare no conflict of interest.

## References

1. Sung, H.; Ferlay, J.; Siegel, R.L.; Laversanne, M.; Soerjomataram, I.; Jemal, A.; Bray, F. Global Cancer Statistics 2020: GLOBOCAN Estimates of Incidence and Mortality Worldwide for 36 Cancers in 185 Countries. *CA Cancer. J. Clin.* **2021**, *71*, 209–249. [[CrossRef](#)] [[PubMed](#)]
2. American College of Radiology ACR BI-RADS Ultrasound. *ACR Breast Imaging Reporting and Data System, Breast Imaging Atlas*, 5th ed.; American College of Radiology: Reston, VA, USA, 2013; pp. 123–132.
3. Bennani-Baiti, B.; Dietzel, M.; Baltzer, P.A. MRI for the Assessment of Malignancy in BI-RADS 4 Mammographic Microcalcifications. *PLoS ONE* **2017**, *12*, e0188679. [[CrossRef](#)]
4. Duffy, S.W.; Smith, R.A.; Gabe, R.; Tabár, L.; Yen, A.M.F.; Chen, T.H.H. Screening for Breast Cancer. *Surg. Oncol. Clin. N. Am.* **2005**, *14*, 671–697. [[CrossRef](#)] [[PubMed](#)]
5. Weinstein, S.P.; Hanna, L.G.; Gatsonis, C.; Schnall, M.D.; Rosen, M.A.; Lehman, C.D. Frequency of Malignancy Seen in Probably Benign Lesions at Contrast-Enhanced Breast MR Imaging: Findings from ACRIN 6667. *Radiology* **2010**, *255*, 731–737. [[CrossRef](#)] [[PubMed](#)]
6. Eby, P.R.; DeMartini, W.B.; Gutierrez, R.L.; Lehman, C.D. Probably Benign Lesions Detected on Breast MR Imaging. *Magn. Reson. Imaging. Clin. N. Am.* **2010**, *18*, 309–321. [[CrossRef](#)]
7. Li, L.; Wang, K.; Sun, X.; Wang, K.; Sun, Y.; Zhang, G.; Shen, B. Parameters of Dynamic Contrast-Enhanced MRI as Imaging Markers for Angiogenesis and Proliferation in Human Breast Cancer. *Med. Sci. Monit.* **2015**, *21*, 376–382. [[CrossRef](#)]
8. Rahbar, H.; Partridge, S.C. Multiparametric MR Imaging of Breast Cancer. *Magn. Reson. Imaging. Clin. N. Am.* **2016**, *24*, 223–238. [[CrossRef](#)]
9. Mann, R.M.; Hooley, R.; Barr, R.G.; Moy, L. Novel Approaches to Screening for Breast Cancer. *Radiology* **2020**, *297*, 266–285. [[CrossRef](#)]
10. Mazaheri, Y.; Afaq, A.; Rowe, D.B.; Lu, Y.; Shukla-Dave, A.; Grover, J. Diffusion-Weighted Magnetic Resonance Imaging of the Prostate: Improved Robustness with Stretched Exponential Modeling. *J. Comput. Assist. Tomogr.* **2012**, *36*, 695–703. [[CrossRef](#)]
11. Le Bihan, D.; Breton, E.; Lallemand, D.; Grenier, P.; Cabanis, E.; Laval-Jeantet, M. MR Imaging of Intravoxel Incoherent Motions: Application to Diffusion and Perfusion in Neurologic Disorders. *Radiology* **1986**, *161*, 401–407. [[CrossRef](#)]
12. Ei Khouli, R.H.; Jacobs, M.A.; Mezban, S.D.; Huang, P.; Kamel, I.R.; Macura, K.J.; Bluemke, D.A. Diffusion-Weighted Imaging Improves the Diagnostic Accuracy of Conventional 3.0-T Breast MR Imaging. *Radiology* **2010**, *256*, 64–73. [[CrossRef](#)] [[PubMed](#)]
13. Mao, X.; Zou, X.; Yu, N.; Jiang, X.; Du, J. Quantitative Evaluation of Intravoxel Incoherent Motion Diffusion-Weighted Imaging (IVIM) for Differential Diagnosis and Grading Prediction of Benign and Malignant Breast Lesions. *Medicine* **2018**, *97*, e11109. [[CrossRef](#)] [[PubMed](#)]

14. Xiao, Z.; Tang, Z.; Qiang, J.; Wang, S.; Qian, W.; Zhong, Y.; Wang, R.; Wang, J.; Wu, L.; Tang, W.; et al. Intravoxel Incoherent Motion MR Imaging in the Differentiation of Benign and Malignant Sinonasal Lesions: Comparison with Conventional Diffusion-Weighted MR Imaging. *AJNR Am. J. Neuroradiol.* **2018**, *39*, 538–546. [[CrossRef](#)] [[PubMed](#)]
15. Ma, W.; Mao, J.; Wang, T.; Huang, Y.; Zhao, Z.H. Distinguishing between Benign and Malignant Breast Lesions Using Diffusion Weighted Imaging and Intravoxel Incoherent Motion: A Systematic Review and Meta-Analysis. *Eur. J. Radiol.* **2021**, *141*, 109809. [[CrossRef](#)] [[PubMed](#)]
16. Sharma, U.; Sah, R.G.; Agarwal, K.; Parshad, R.; Seenu, V.; Mathur, S.R.; Hari, S.; Jagannathan, N.R. Potential of Diffusion-Weighted Imaging in the Characterization of Malignant, Benign, and Healthy Breast Tissues and Molecular Subtypes of Breast Cancer. *Front. Oncol.* **2016**, *6*, 126. [[CrossRef](#)] [[PubMed](#)]
17. Liu, C.; Liang, C.; Liu, Z.; Zhang, S.; Huang, B. Intravoxel Incoherent Motion (IVIM) in Evaluation of Breast Lesions: Comparison with Conventional DWI. *Eur. J. Radiol.* **2013**, *82*, e782–e789. [[CrossRef](#)]
18. Tan, P.H.; Ellis, I.; Allison, K.; Brogi, E.; Fox, S.B.; Lakhani, S.; Lazar, A.J.; Morris, E.A.; Sahin, A.; Salgado, R.; et al. The 2019 World Health Organization Classification of Tumours of the Breast. *Histopathology* **2020**, *77*, 181–185. [[CrossRef](#)]
19. Le Bihan, D.; Turner, R.; MacFall, J.R. Effects of Intravoxel Incoherent Motions (IVIM) in Steady-State Free Precession (SSFP) Imaging: Application to Molecular Diffusion Imaging. *Magn. Reson. Med.* **1989**, *10*, 324–337. [[CrossRef](#)]
20. Bakker, M.F.; de Lange, S.V.; Pijnappel, R.M.; Mann, R.M.; Peeters, P.H.M.; Monninkhof, E.M.; Emaus, M.J.; Loo, C.E.; Bisschops, R.H.C.; Lobbes, M.B.I.; et al. Supplemental MRI Screening for Women with Extremely Dense Breast Tissue. *N. Engl. J. Med.* **2019**, *381*, 2091–2102. [[CrossRef](#)]
21. Liu, Z.; Wang, S.; Dong, D.; Wei, J.; Fang, C.; Zhou, X.; Sun, K.; Li, L.; Li, B.; Wang, M.; et al. The Applications of Radiomics in Precision Diagnosis and Treatment of Oncology: Opportunities and Challenges. *Theranostics* **2019**, *9*, 1303–1322. [[CrossRef](#)]
22. Thibault, G.; Fertil, B.; Navarro, C.; Pereira, S.; Cau, P.; Levy, N.; Sequeira, J.; Mari, J.-L. Shape and Texture Indexes Application to Cell Nuclei Classification. *Int. J. Pattern Recogn. Artif. Intell.* **2013**, *27*, 1357002. [[CrossRef](#)]
23. Thibault, G.; Angulo, J.; Meyer, F. Advanced Statistical Matrices for Texture Characterization: Application to Cell Classification. *IEEE. Trans. Biomed. Eng.* **2014**, *61*, 630–637. [[CrossRef](#)] [[PubMed](#)]
24. Hall-Beyer, M. *GLCM Texture: A Tutorial v. 3.0 March 2017*; University of Calgary Press: Calgary, AB, Canada, 2017. [[CrossRef](#)]
25. Jiang, Y.; Edwards, A.V.; Newstead, G.M. Artificial Intelligence Applied to Breast MRI for Improved Diagnosis. *Radiology* **2021**, *298*, 38–46. [[CrossRef](#)]
26. Partridge, S.C.; Nissan, N.; Rahbar, H.; Kitsch, A.E.; Sigmund, E.E. Diffusion-Weighted Breast MRI: Clinical Applications and Emerging Techniques. *J. Magn. Reson. Imaging* **2017**, *45*, 337–355. [[CrossRef](#)] [[PubMed](#)]
27. Sun, S.Y.; Ding, Y.; Li, Z.; Nie, L.; Liao, C.; Liu, Y.; Zhang, J.; Zhang, D. Multiparameter MRI Model With DCE-MRI, DWI, and Synthetic MRI Improves the Diagnostic Performance of BI-RADS 4 Lesions. *Front. Oncol.* **2021**, *11*, 699127. [[CrossRef](#)] [[PubMed](#)]
28. Zhang, L.; Tang, M.; Min, Z.; Lu, J.; Lei, X.; Zhang, X. Accuracy of Combined Dynamic Contrast-Enhanced Magnetic Resonance Imaging and Diffusion-Weighted Imaging for Breast Cancer Detection: A Meta-Analysis. *Acta. Radiol.* **2016**, *57*, 651–660. [[CrossRef](#)] [[PubMed](#)]
29. Ma, Y.; Shan, D.; Wei, J.; Chen, A. Application of Intravoxel Incoherent Motion Diffusion-Weighted Imaging in Differential Diagnosis and Molecular Subtype Analysis of Breast Cancer. *Am. J. Transl. Res.* **2021**, *13*, 3034–3043.
30. Meng, N.; Wang, X.-J.; Sun, J.; Huang, L.; Wang, Z.; Wang, K.-Y.; Wang, J.; Han, D.-M.; Wang, M.-Y. Comparative Study of Amide Proton Transfer-Weighted Imaging and Intravoxel Incoherent Motion Imaging in Breast Cancer Diagnosis and Evaluation. *J. Magn. Reson. Imaging* **2020**, *52*, 1175–1186. [[CrossRef](#)]
31. Liang, J.; Zeng, S.; Li, Z.; Kong, Y.; Meng, T.; Zhou, C.; Chen, J.; Wu, Y.; He, N. Intravoxel Incoherent Motion Diffusion-Weighted Imaging for Quantitative Differentiation of Breast Tumors: A Meta-Analysis. *Front. Oncol.* **2020**, *10*, 585486. [[CrossRef](#)]
32. Wang, Q.; Wang, D.; Zhang, J.; Huang, M.; Guo, Y.; Wang, Z. Influence of age and menstrual statuses on breast intravoxel incoherent motion imaging. *Chin. J. Clin.* **2015**, *17*, 3238–3243. [[CrossRef](#)]
33. Kim, S.H.; Lee, H.S.; Kang, B.J.; Song, B.J.; Kim, H.-B.; Lee, H.; Jin, M.-S.; Lee, A. Dynamic Contrast-Enhanced MRI Perfusion Parameters as Imaging Biomarkers of Angiogenesis. *PLoS ONE* **2016**, *11*, e0168632. [[CrossRef](#)] [[PubMed](#)]
34. El Khouli, R.H.; Macura, K.J.; Kamel, I.R.; Jacobs, M.A.; Bluemke, D.A. 3-T Dynamic Contrast-Enhanced MRI of the Breast: Pharmacokinetic Parameters versus Conventional Kinetic Curve Analysis. *Am. J. Roentgenol.* **2011**, *197*, 1498–1505. [[CrossRef](#)]
35. Yao, W.W.; Zhang, H.; Ding, B.; Fu, T.; Jia, H.; Pang, L.; Song, L.; Xu, W.; Song, Q.; Chen, K.; et al. Rectal Cancer: 3D Dynamic Contrast-Enhanced MRI; Correlation with Microvascular Density and Clinicopathological Features. *Radiol. Med.* **2011**, *116*, 366–374. [[CrossRef](#)] [[PubMed](#)]
36. Li, S.P.; Padhani, A.R.; Taylor, N.J.; Beresford, M.J.; Ah-See, M.-L.W.; Stirling, J.J.; d’Arcy, J.A.; Collins, D.J.; Makris, A. Vascular Characterisation of Triple Negative Breast Carcinomas Using Dynamic MRI. *Eur. Radiol.* **2011**, *21*, 1364–1373. [[CrossRef](#)] [[PubMed](#)]
37. Iima, M.; Kataoka, M.; Kanao, S.; Onishi, N.; Kawai, M.; Ohashi, A.; Sakaguchi, R.; Toi, M.; Togashi, K. Intravoxel Incoherent Motion and Quantitative Non-Gaussian Diffusion MR Imaging: Evaluation of the Diagnostic and Prognostic Value of Several Markers of Malignant and Benign Breast Lesions. *Radiology* **2018**, *287*, 432–441. [[CrossRef](#)] [[PubMed](#)]

- 
38. Baxter, G.C.; Graves, M.J.; Gilbert, F.J.; Patterson, A.J. A Meta-Analysis of the Diagnostic Performance of Diffusion MRI for Breast Lesion Characterization. *Radiology* **2019**, *291*, 632–641. [[CrossRef](#)]
  39. Li, K.; Machireddy, A.; Tudorica, A.; Moloney, B.; Oh, K.Y.; Jafarian, N.; Partridge, S.C.; Li, X.; Huang, W. Discrimination of Malignant and Benign Breast Lesions Using Quantitative Multiparametric MRI: A Preliminary Study. *Tomography* **2020**, *6*, 148–159. [[CrossRef](#)]